Original article

Nuclear Medicine Communications

Performance evaluation of kinetic parameter estimation methods in dynamic FDG-PET studies

Xiaoqian Dai, Zhe Chen and Jie Tian

Purpose **To evaluate several popular parameter estimation methods for determining the cerebral metabolic rate for glucose and individual kinetic rate constant parameters in 2-deoxy-2-[^{18}F]fluoro-D-glucose positron emission tomography studies.**

Procedures **These methods can be divided into two categories: nonlinear estimation methods and linear estimation methods. The nonlinear estimation methods include nonlinear least squares (NLLS), weighted NLLS using noisy tissue time-activity data (WNLLS-N), weighted NLLS using noise-free tissue time-activity data (WNLLS-NF), iteratively reweighted NNLS (IRWNLLS) and nonlinear ridge regression (NLRR) method, whereas the linear estimation methods include Patlak–Gjedde graphical analysis (PGA), linear least squares (LLS), generalized LLS (GLLS), total least squares (TLS) and the basis functions (BF) method. Simulation studies are presented.**

Results and conclusion **There are several findings: (i) when the noise level is low, GLLS performs well. However, it exhibits large bias and poor precision especially in k_3^* and k_4^* when the noise level is high. (ii) BF is a promising method with superior bias and precision properties, and is less affected by the scan duration used. (iii) The weighting factors in the nonlinear estimation methods are important: a good choice of weights can help to make the estimates more accurate and reliable. Weighting based on noisy data should be avoided. (iv) It confirms that PGA is little affected by noise, but the assumptions of PGA could induce bias. It also confirms that 60 min is not long enough to give reliable estimates of k_4^* especially for the linear estimation methods LLS, TLS, and GLLS.** *Nucl Med Commun* **32:4–16 © 2011 Wolters Kluwer Health | Lippincott Williams & Wilkins.**

Nuclear Medicine Communications 2011, **32**:4–16

Keywords: 2-deoxy-2-[^{18}F]fluoro-D-glucose, linear estimation methods, nonlinear estimation methods, parameter estimation, positron emission tomography

Medical Image Processing Group, Institute of Automation, Chinese Academy of Sciences, Beijing, China

Correspondence to Jie Tian, PhD, Medical Image Processing Group, Institute of Automation, Chinese Academy of Sciences, No. 95 Zhongguancun East Road, Beijing 100190, China
Tel: +86 10 82628760; fax: +86 10 62527995;
e-mail: tian@ieee.org; jie.tian@ ia.ac.cn

Received 15 June 2010 **Revised** 15 August 2010
Accepted 16 August 2010

Introduction

2-Deoxy-2-[^{18}F]fluoro-D-glucose positron emission tomography (^{18}F-FDG PET) has played an important role in quantitatively estimating physiological parameters of the human brain such as the cerebral metabolic rate for glucose (MRGlc) [1]. Measurement of these physiological parameters can provide a clear insight into the underlying processes in the human brain to help with a more accurate diagnosis. Traditionally, to determine the parameters, the acquired tissue time–activity curves (TTACs) from a dynamic ^{18}F-FDG PET scan and the measured tracer concentration in blood/plasma over the duration of the scan, are fitted to the appropriate tracer kinetic model. The model-fitting methods to estimate the parameters can be roughly divided into two categories: nonlinear estimation methods and linear estimation methods.

The classical nonlinear estimation methods are considered to be the methods with optimum statistical accuracy as the solution of the ^{18}F-FDG kinetic model is nonlinear and the fitting procedure is iterative. These nonlinear estimation methods are based on the maximum-likelihood principle and use nonlinear optimization to estimate parameter values [2]. The gold standard nonlinear estimation method is the nonlinear least squares method (NLLS), in which the objective function to be minimized is the residual sum of squares. Sometimes a modified objective function is minimized, wherein each of the squared deviations is multiplied by a weighting factor. A proper choice of weights could emphasize the precise parts of the data and reduce the importance of the questionable parts of the data, thus helping to improve the estimation accuracy. To investigate the effect of different weights, the NLLS method, which can be regarded as a unit-weighted method, the iteratively reweighted NLLS (IRWNLLS) method, the weighted NLLS using noisy tissue time-activity data (WNLLS-N) and the weighted NLLS using noise-free tissue time-activity data (WNLLS-NF) were evaluated in this study. In addition, a recently proposed nonlinear ridge regression method (NLRR) [3,4], which makes use of prior information by adding a penalty function to the objective function of NLLS, was also included for comparison.

All supplementary data are available directly from the authors.

0143-3636 © 2010 Wolters Kluwer Health | Lippincott Williams & Wilkins

DOI: 10.1097/MNM.0b013e32833f6c05

Although in theory, nonlinear estimation methods can be applied to obtain parametric images on a voxel-by-voxel basis, they suffer from too much computational burden and may be prone to trapping in local minima. Thus, alternative methods were proposed. In the category of linear estimation methods, the Patlak–Gjedde graphical analysis (PGA) method [5,6] is widely used in dynamic PET data analysis for determining the MRGlc because of its simplicity and computational efficiency. However, it has been pointed out [7] that the MRGlc is often underestimated because of the assumption of an irreversible model (i.e. $k_4^* = 0$). Blomqvist [8] proposed the linear least squares (LLS) method, which was later extended to ^{18}F-FDG tracer by Evans *et al.* [9]. However, bias exists in parameters estimated from LLS because of the noise present in TTACs that propagates as correlated error in the right side of the LLS equation [7,10]. To overcome this problem, the generalized LLS (GLLS) method [10,11] was proposed. It incorporates an autoregressive model for the noise into the estimation process to turn the correlated noise into white noise, thus to reduce the bias. The total least squares (TLS) [12] method (also called perpendicular linear regression), in which observational errors on dependent and independent variables are both taken into account, has been applied to parametric imaging in the field of nuclear medicine recently [13–15].

Spectral analysis was first introduced in the field of dynamic PET studies by Cunningham and Jones [16], and was then successfully applied to many tracer studies [17–20]. The technique uses a set of basis functions (BF) that enables the incorporation of parameter bounds to linearize the solution of the kinetic model. Hong and Fryer [21] have extended this BF technique to a two-compartment model and applied it to ^{18}F-FDG tracer.

In this study, the methods mentioned earlier, including the five types of nonlinear estimation methods and the five types of linear estimation methods, were systematically compared and evaluated. The aim of this study was to further evaluate the accuracy and precision of these methods for determining the kinetic rate constants and the MRGlc. Only simulation studies were presented as the true values could be obtained for accurate comparison. Different noise levels were investigated to evaluate the performance of each method as a function of noise. The effects of different scanning sequences were also taken into account.

Methods

The 2-deoxy-2-[^{18}F]fluoro-D-glucose model

The commonly used three-compartment, five-parameter model [1,22] is used to describe the rates of changes in concentration in the brain:

$$\begin{cases} \frac{d}{dt}C_e^*(t) = K_1^* C_p{}^*(t) - (k_2^* + k_3^*)C_e^*(t) + k_4^* C_m^*(t) \\ \frac{d}{dt}C_m^*(t) = k_3^* C_e^*(t) - k_4^* C_m^*(t) \end{cases} \quad (1)$$
$$C_i^*(t) = (1 - V_b)(C_e^*(t) + C_m^*(t)) + V_b C_p^*(t)$$

in which $C_p^*(t), C_e^*(t)$, and $C_m^*(t)$, are the ^{18}F-FDG concentration in plasma, the concentration of free ^{18}F-FDG in tissue, and the concentration of ^{18}F-FDG-6-phosphate in tissue. $C_p^*(t)$ is obtained from blood samples, whereas the sum of the activity in the tissue $C_i^*(t)$ is obtained from PET scan measurements. K_1^* is the forward transport rate constant of ^{18}F-FDG from the plasma to the tissue, k_2^* is the reversed transport rate constant from the tissue back to the plasma, k_3^* is the phosphorylation rate constant, k_4^* is the dephosphorylation rate constant, and V_b is the fractional blood volume of the tissue. Denote $\theta = [K_1^*, k_2^*, k_3^*, k_4^*, V_b]$ as the parameter set to be estimated. Once the parameters are obtained, MRGlc can be calculated by:

$$\mathrm{MRGlc} = \frac{C_p}{\mathrm{LC}} \cdot \frac{K_1^* k_3^*}{k_2^* + k_3^*} \equiv \frac{C_p}{\mathrm{LC}} \cdot \mathrm{K} \quad (2)$$

in which C_p is the glucose concentration in plasma. The lumped constant (LC) is usually defined as a constant.

The noise model of tissue time–activity curves

As noise was present in the real measured PET data, a commonly used noise model was used to simulate the measurement noise in the simulation study. The noise model adopted here has been used extensively by several other researchers [7,15,23].

Here, noise was added to a simulated noise-free PET TTAC using:

$$C_i^*(t_k) = C_i^{*0}(t_k) + \sigma(t_k) * N(0,1) \quad (3)$$

in which $C_i^{*0}(t_k)$ is the simulated noise-free TTAC and $C_i^*(t_k)$ is the simulated noisy TTAC. N (0,1) stands for a pseudo-random number generated from normal distribution (Gaussian distribution) with zero mean and a standard deviation of one. The measurement noise standard deviation (decay corrected) $\sigma(t_k)$ is accurately modeled using the following equation:

$$\sigma(t_k) = \alpha \sqrt{\frac{C_i^{*0}(t_k) \cdot e^{\lambda t_k}}{\Delta t_k}} \quad (4)$$

in which the coefficient α is a proportionality constant that actually determines the noise level in the simulation study, Δt_k is the k^{th} frame length, and λ is the decay constant of the isotope ^{18}F that can be calculated from the half-life of ^{18}F, ($t_{1/2}$), from equation $\lambda = \ln 2/t_{1/2}$. In this study, α was set to 0, 0.2, 0.4, 0.6, and 0.8, in which 0

corresponds to no noise added and 0.4 is approximately the clinical noise level [21].

The nonlinear estimation methods

Nonlinear least squares method

The solution of equations (1) can be derived by Laplace transforms and further rearranged as:

$$C_i^*(t) = \frac{(1-V_b)K_1^*}{\alpha_2-\alpha_1}\{(k_3^*+k_4^*-\alpha_1)e^{-\alpha_1 t} + (\alpha_2-k_3^*-k_4^*)e^{-\alpha_2 t}\} \otimes C_p^*(t) + V_b C_p^*(t) \quad (5)$$

where $\alpha_1 = (k_2^*+k_3^*+k_4^* - \sqrt{(k_2^*+k_3^*+k_4^*)^2 - 4k_2^*k_4^*})/2$,

and $\alpha_2 = (k_2^*+k_3^*+k_4^* + \sqrt{(k_2^*+k_3^*+k_4^*)^2 - 4k_2^*k_4^*})/2$.

Parameter estimation using NLLS requires nonlinear regression of the objective function:

$$\mathrm{RSS}(\theta) = \sum_{k=1}^{N} [\tilde{C}_i^*(t_k) - C_i^*(t_k)]^2 \quad (6)$$

in which $\mathrm{RSS}(\theta)$ stands for the residual sum of squares between the estimated TTAC $\tilde{C}_i^*(t_k)$ and the simulated TTAC $C_i^*(t_k)$ [see equation (3)]. NLLS can be regarded as a WNLLS method with equal weights.

Weighted nonlinear least squares methods using noise-free tissue time–activity data

In WNLLS-NF, the values of the parameters are estimated by minimizing the objective function:

$$\mathrm{WRSS}(\theta) = \sum_{k=1}^{N} \omega_{t_k} [\tilde{C}_i^*(t_k) - C_i^*(t_k)]^2 \quad (7)$$

in which $\mathrm{WRSS}(\theta)$ stands for the weighted residual sum of squares. The weighting factor ω_{t_k} reflects the relative accuracy of the measurement at time t_k. Here the weights ω_{t_k} are set equal to the inverse of the ideal noise variance, that is, $\omega_{t_k} = 1/\sigma(t_k)^2$, with

$$\sigma(t_k) = \alpha[C_i^{*0}(t_k) \cdot e^{\lambda t_k}/(\Delta t_k)]^{0.5} \quad (8)$$

in which the $C_i^{*0}(t_k)$ is the k^{th} simulated noise-free TTAC [see equation (3)]. It should be noted that the weighting factors in WNLLS-NF are calculated using the ideal noise-free TTAC $C_i^{*0}(t_k)$. Therefore, in theory, WNLLS-NF can obtain the smallest variance of estimates.

Weighted nonlinear least squares method using noisy tissue time–activity data

When the WNLLS-N method is used, the object function is also expressed by equation (7), however, with

$$\sigma(t_k) = \alpha[C_i^*(t_k) \cdot e^{\lambda t_k}/(\Delta t_k)]^{0.5} \quad (9)$$

in which $C_i^*(t_k)$ is the k^{th} simulated noisy tissue time-activity data [see equation (3)].

WNLLS-N is the most often used nonlinear estimation method in practice. Compared with equation (4), WNLLS-N uses the noisy TTAC $C_i^*(t_k)$ to calculate the noise variance to approach the 'true' noise variance.

Iteratively reweighted nonlinear least squares method

In the IRWNLLS method, the objective function is also expressed by equation (7), with the standard deviation σ calculated each time from the new estimated TTAC $\tilde{C}_i^*(t_k)$:

$$\sigma(t_k) = \alpha[\tilde{C}_i^*(t_k) \cdot e^{\lambda t_k}/(\Delta t_k)]^{0.5} \quad (10)$$

The process iterates until the estimated parameter set $\theta = [K_1^*, k_2^*, k_3^*, k_4^*, V_b]$ converges.

Nonlinear ridge regression method

In NLRR method, the objective function is given by Byrtek *et al.* [3] and O'sullivan and Saha [4]:

$$O_{\mathrm{NLRR}}(\theta) = \mathrm{WRSS}(\theta) + \tau(\theta-\mu)' \sum\nolimits_{\theta}^{-1} (\theta-\mu) \quad (11)$$

in which τ is the ridge biasing parameter that determines the degree of emphasis on the penalty term, μ is a set of physiologically reasonable values for θ, and $\sum_\theta$ is a diagonal matrix that scales the deviation of θ from μ.

The linear estimation methods

The Patlak–Gjedde graphical analysis method

The PGA has been developed for an irreversible model, in which k_4^* is assumed to be zero. The PGA solution to the ^{18}F-FDG model (1) under a steady-state condition [6] is given by the expression:

$$\frac{C_i^*(t)}{C_p^*(t)} = \mathrm{K} \cdot \frac{\int_0^t C_p^*(\tau)d\tau}{C_p^*(t)} + V \quad (12)$$

in which the slope K and the intercept V can be obtained by linear regression from a graph of $C_i^*(t)/C_p^*(t)$ against $\int_0^t C_p^*(\tau)d\tau/C_p^*(t)$. The PGA method is easy to implement and is computationally efficient; however, it cannot estimate the individual rate constants, and the assumption of the irreversible model may induce large bias in the estimated MRGlc.

Linear least squares method

The solution of the ^{18}F-FDG model (1), can be derived by converting (1) into the following linear equation [10]:

$$C_i^*(t) = P_1 C_p^*(t) + P_2 \int_0^t C_P^*(\tau)d\tau + P_3 \int_0^t \int_0^\tau C_P^*(\tau)d\tau^2 + P_4 \int_0^t C_i^*(\tau)d\tau + P_5 \int_0^t \int_0^\tau C_i^*(\tau)d\tau^2 \quad (13)$$

in which $P_1 = V_b$, $P_2 = (k_2^* + k_3^* + k_4^* - K_1^*) \cdot V_b + K_1^*$, $P_3 = (k_2^* k_4^* - K_1^* k_3^* - K_1^* k_4^*) \cdot V_b + K_1^*(k_3^* + k_4^*)$, $P_4 = -(k_2^* + k_3^* + k_4^*)$, $P_5 = -k_2^* k_4^*$. Digitize the equation at each sample time of the tissue measurements t_k ($k = 1, 2, \ldots, m$), and then rearrange them into a matrix form:

$$y = XP + \varepsilon \quad (14)$$

in which $y = [C_i^*(t_1)\, C_i^*(t_2) \ldots C_i^*(t_m)]^T$, $P = [P_1 \;\; P_2 \;\; \ldots \;\; P_5]^T$, $\varepsilon = [\varepsilon_1\, \varepsilon_2 \ldots \varepsilon_m]^T$ are the equation error terms, X is the coefficient matrix:

$$X = \begin{bmatrix} C_p^*(t_1) + \hat{P}_4\psi_1 \otimes C_p^*(t_1) + \hat{P}_5\psi_2 \otimes C_i^*(t_1) & \psi_1 \otimes C_p^*(t_1) & \psi_2 \otimes C_p^*(t_1) & \psi_1 \otimes C_i^*(t_1) & \psi_2 \otimes C_i^*(t_1) \\ C_p^*(t_2) + \hat{P}_4\psi_1 \otimes C_p^*(t_2) + \hat{P}_5\psi_2 \otimes C_i^*(t_2) & \psi_1 \otimes C_p^*(t_2) & \psi_2 \otimes C_p^*(t_2) & \psi \otimes C_i^*(t_2) & \psi_2 \otimes C_i^*(t_2) \\ \vdots & \vdots & \vdots & \vdots & \vdots \\ C_p^*(t_m) + \hat{P}_4\psi_1 \otimes C_p^*(t_m) + \hat{P}_5\psi_2 \otimes C_i^*(t_m) & \psi_1 \otimes C_p^*(t_m) & \psi_2 \otimes C_p^*(t_m) & \psi_1 \otimes C_i^*(t_m) & \psi_2 \otimes C_i^*(t_m) \end{bmatrix},$$

$$X = \begin{bmatrix} C_p^*(t_1) & \int_0^{t_1} C_p^*(\tau)d\tau & \int_0^{t_1}\int_0^\tau C_p^*(\tau)d\tau^2 & \int_0^{t_1} C_i^*(\tau)d\tau & \int_0^{t_1}\int_0^\tau C_i^*(\tau)d\tau^2 \\ C_p^*(t_2) & \int_0^{t_2} C_p^*(\tau)d\tau & \int_0^{t_2}\int_0^\tau C_p^*(\tau)d\tau^2 & \int_0^{t_2} C_i^*(\tau)d\tau & \int_0^{t_2}\int_0^\tau C_i^*(\tau)d\tau^2 \\ \vdots & \vdots & \vdots & \vdots & \vdots \\ C_p^*(t_m) & \int_0^{t_m} C_p^*(\tau)d\tau & \int_0^{t_m}\int_0^\tau C_p^*(\tau)d\tau^2 & \int_0^{t_m} C_i^*(\tau)d\tau & \int_0^{t_m}\int_0^\tau C_i^*(\tau)d\tau^2 \end{bmatrix}.$$

The solution can be obtained from:

$$\hat{P}_{\mathrm{LLS}} = (X^T X)^{-1} X^T y \quad (15)$$

Once the estimates for $\hat{P}_{\mathrm{LLS}}$ have been obtained, the rate constants, $K_1^* - k_4^*$ and V_b can be calculated by:

$$K_1^* = \frac{P_1 P_4 + P_2}{1 - P_1};\; k_2^* = \frac{P_1 P_5 + P_3}{P_1 P_4 + P_2} - P_4; \quad k_3^* = -(k_2^* + k_3^* + P_4);\; k_4^* = -\frac{P_5}{k_2^*};\; V_b = P_1 \quad (16)$$

It has been reported that because of the presence of the noisy term on both sides of equation (13), the errors in equation (14) are correlated as they consist of the direct measurement noise and integrals of the measurement noise. Therefore, the equation errors ε are not statistically independent, which is the cause of correlated errors leading to bias in parameter estimations [7,10].

Generalized linear least squares method

GLLS is developed to overcome the shortcoming of LLS by whitening the correlated equation noises iteratively. The detailed description of GLLS has been presented by Feng *et al.* [7,11] and Cai *et al.* [10]. The solution can be obtained by:

$$\hat{P}_{\mathrm{GLLS}} = (X^T X)^{-1} X^T y \quad (17)$$

in which

$$y = \begin{bmatrix} C_i^*(t_1) + \hat{P}_4\psi_1 \otimes C_i^*(t_1) + \hat{P}_5\psi_2 \otimes C_i^*(t_1) \\ C_i^*(t_2) + \hat{P}_4\psi_1 \otimes C_i^*(t_2) + \hat{P}_5\psi_2 \otimes C_i^*(t_2) \\ \vdots \\ C_i^*(t_m) + \hat{P}_4\psi_1 \otimes C_i^*(t_m) + \hat{P}_5\psi_2 \otimes C_i^*(t_m) \end{bmatrix},$$

with $\psi_1 = \dfrac{1}{\lambda_2 - \lambda_1}(\lambda_2 e^{-\lambda_2 t} - \lambda_1 e^{-\lambda_1 t})$,

$$\psi_2 = \frac{1}{\lambda_2 - \lambda_1}(e^{-\lambda_1 t} - e^{-\lambda_2 t}),\; \lambda_1 = -\frac{\hat{P}_4 + \sqrt{\hat{P}_4^2 + 4\hat{P}_5^2}}{2},$$

$$\lambda_2 = -\frac{\hat{P}_4 - \sqrt{\hat{P}_4^2 + 4\hat{P}_5^2}}{2}.$$

The iteration stops when the parameter estimates converge. After the estimates for $\hat{P}_{\mathrm{GLLS}}$ have been obtained, the parameter set θ can be calculated using equation (16).

Total least squares method

The TLS method considers that both sides of equation (14) have noise, and then the equation in LLS can be refined as:

$$y + \varepsilon = (X + E)P \quad (18)$$

in which ε and E are error matrices. The aim is to find P that minimizes error matrices ε and E for y and X, respectively, that is, $\mathrm{argmin}_{\varepsilon,E}||[\varepsilon, E]||_\varepsilon$. Using singular value decomposition: $[(X+E) \quad (y+\varepsilon)] = [U_X \quad U_y] \begin{bmatrix} \Sigma_X & 0 \\ 0 & \Sigma_y \end{bmatrix} \begin{bmatrix} V_{XX} & V_{Xy} \\ V_{yX} & V_{yy} \end{bmatrix}^*$, and then the solution can be obtained by:

$$\hat{P}_{\mathrm{TLS}} = -V_{Xy} V_{yy}^{-1} \quad (19)$$

Once the estimates for $\hat{P}_{\mathrm{TLS}}$ have been obtained, θ can be calculated using equation (16).

The basis functions method

The detailed description of the BF method has been presented by Hong and Fryer [21]. In this method, equation (5) can be rewritten as:

$$C_i^*(t) = (\theta_1 e^{-\alpha_1 t} + \theta_2 e^{-\alpha_2 t}) \otimes C_p^*(t) + V_b C_p^*(t) \qquad (20)$$

Through linearization of the convolution term, a set of BF can be obtained:

$$B_{ij}(t) = e^{-\alpha_{ij} t} \otimes C_p^*(t) \quad i = 1, 2; \quad j = 1, \ldots, N \qquad (21)$$

in which N is the number of the basis functions. Then for each basis function, the model can be rewritten as:

$$C_i^*(t) = \theta_1 B_{1j} + \theta_2 B_{2l} + V_b C_p^*(t) \quad j, l = 1, 2, \ldots, N \quad (22)$$

The parameters (θ_1, θ_2, V_b) can then be solved by using the linear regression method for each basis function. The parameter set with the lowest weighted residual sum of squares is chosen as the solution. Then the rate constants, $K_1^* - k_4^* (k_4^* \neq 0)$ can be obtained from:

$$\begin{aligned} K_1^* &= \frac{\theta_1 + \theta_2}{1 - V_b}, \; k_2^* = \frac{\theta_1 \alpha_1 + \theta_2 \alpha_2}{\theta_1 + \theta_2}, \\ k_3^* &= \frac{\alpha_1 \alpha_2 (\theta_1 + \theta_2)}{\theta_1 \alpha_1 + \theta_2 \alpha_2}, \; k_4^* = \frac{\theta_1 \theta_2 (\alpha_2 - \alpha_1)^2}{(\theta_1 + \theta_2)(\theta_1 \alpha_1 + \theta_2 \alpha_2)} \end{aligned} \qquad (23)$$

Simulation study

The plasma time–activity curve

In the simulation study, the plasma time–activity curve (PTAC) was modeled using the method proposed by Feng *et al.* [24]:

$$C_p^*(t) = [A_1 t - A_2 - A_3] e^{\lambda_1 t} + A_2 e^{\lambda_2 t} + A_3 e^{\lambda_3 t} \qquad (24)$$

in which A_1, A_2, and A_3 are the coefficients and λ_1, λ_2, and λ_3 are the eigenvalues. A typical parameter set used here was [7]: $A_1 = 851.1225$, $A_2 = 20.8113$, $A_3 = 21.8798$ (μCi/ml), $\lambda_1 = -4.1339$, $\lambda_2 = -0.0104$, $\lambda_3 = -0.1191$ (l/min). The delay was not modeled. We assumed that no errors occurred in the PTAC as we focused our attention on the effects of PET measurement noise on the various parameter estimation methods. The sample times were 8×15, 2×30 s, 4, 5, 7, 10, 15, and every 10 min thereafter.

The tissue time–activity curves

The TTACs were modeled using equation (3) with noise variance modeled using equation (4). One set of parameters from the literature published earlier was used here [1,7]: $K_1^* = 0.1020$, $k_2^* = 0.1300$, $k_3^* = 0.0620$, $k_4^* = 0.0068$ and $V_b = 0.058$ with $C_\mathrm{p} = 91.9$ mg/100 ml and LC = 0.418. To account for the effect of different scanning sequences, two PET scanning schedules were simulated: 8×15, 4×30, 6×60, 6×150, 7×300 s for the 60 min scans [21] and 10×12, 2×30, 2×60, 1×90, 1×210, 2×300, 1×600, 3×1800 s for the 120 min scans [7].

Configuration and evaluation criteria

In all nonlinear estimation methods, the lower bound and upper bound constraints were: $\mathrm{LB}_\theta = [0.01, 0.01, 0.001, 0.001, 0.001]$ and $\mathrm{UB}_\theta = [2.0, 1.0, 1.0, 0.1, 0.1]$. The initial values for all the nonlinear estimation methods were obtained using LLS. For all cases, *fmincon* from MATLAB was used to minimize the objective functions. In IRWNLLS, the number of reweighting iterations was set to a maximum of 20. In NLRR, μ was set to the true parameter values and τ was estimated by a plug-in strategy [4], that is, $\tau = p\hat{\sigma}^2 / ||[\hat{\theta}(0) - \mu]||^2$, where $\hat{\sigma} = 1/(N-p)\mathrm{WRSS}[\hat{\theta}(0)]$, in which $\hat{\theta}(0)$ is the LLS estimate, p is the number of estimated parameters. The matrix $\sum_\theta$ was estimated using: $\Sigma_\theta^{-1} = v_j/\mu_j$, in which v_j and μ_j is the coefficient of variation (CV) and the mean taken over a number of patients from Dr Spence's laboratory [4].

In the category of linear estimation methods, the PGA method uses TTACs from 20 min onwards to fit transformed data to a line. For the GLLS method, the initial values were from the estimates using LLS, and only two iterations were implemented, as in most cases (more than 80%) two iterations were enough to converge, which is consistent with that of Feng *et al.* [7]. In BF, the ranges of physiological values used for α_1 and α_2 are: 100 logarithmically spaced $\alpha_1 \in [0.0005, 0.015]$/min and $\alpha_2 \in [0.06, 0.6]$/min [21].

In this study, box plots were used to show the distribution of parameters estimated from these different methods. The box plots depict the data through four statistical measures: the median (50th percentile of the data), the upper (75th percentile of the data) and lower (25th percentile of the data) quartiles and the outliers beyond 1.5 times interquartile range (IQR, i.e. 25–75th percentile of the data) in each direction. The box plots can provide simply but directly a graphical summary of the location and dispersion of the data. For better understanding of the data, accuracy and precision of the estimates obtained by each analysis method were also provided for comparison. Percentage bias for each parameter was calculated to evaluate the accuracy of the estimates, with $\mathrm{Bias} = (1/M)\Sigma_{i=1}^{M}(p_i - p_o)/p_o * 100\%$, in which M is the number of realizations, p_i is the estimated parameter value, and p_o is the corresponding true parameter value. The CV of the estimates was calculated to describe the precision of each method as a function of noise. CV is the ratio of the standard deviation to the mean, that is, $\mathrm{CV} = \sigma/\mu$. CV is a normalized measure of dispersion of a variable that does not depend

Fig. 1

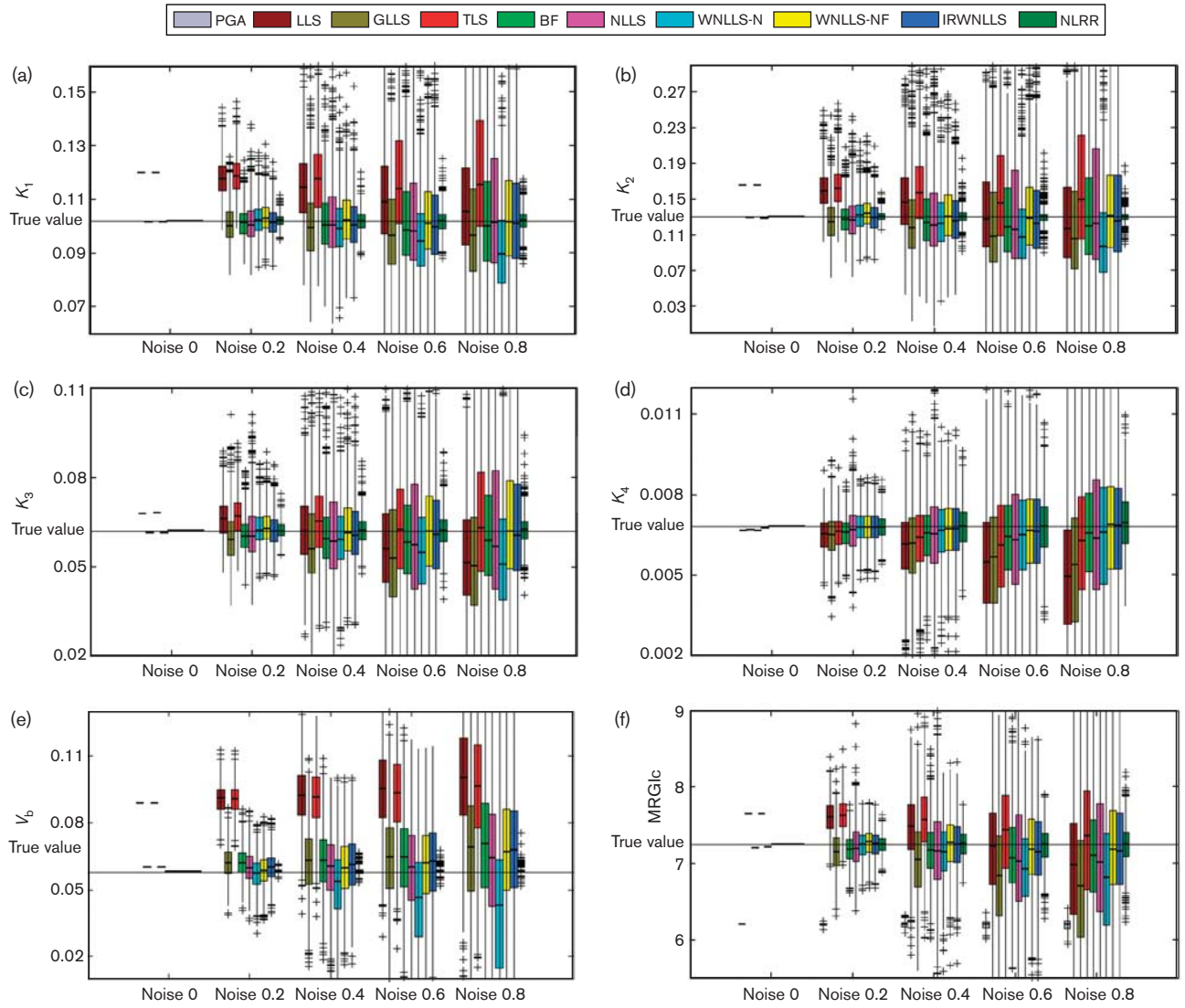

Box plots of (a)K_1^*, (b) k_2^*, (c) k_3^*, (d) k_4^*, (e) V_b, and (f) metabolic rate for glucose (MRGlc) estimates obtained with different methods at different noise levels. The scanning length is 120 min. The individual boxes have lines at the lower, median and upper quartile values. The whiskers extend from the ends of the box to the most extreme value with 1.5 times the interquartile range in each direction. The estimates beyond the whiskers are marked as outliers (denoted by '+'). The true value of the used parameter set is $\theta = [K_1^*, k_2^*, k_3^*, k_4^*, V_b] = [0.1020, 0.1300, 0.0620, 0.0068, 0.058]$. BF, basis functions; GLLS, generalized linear least squares; IRWNLLS, iteratively reweighted nonlinear least squares; LLS, linear least squares; NLLS, nonlinear least squares; NLRR, nonlinear ridge regression; PGA, Patlak–Gjedde graphical analysis; TLS, total least squares;WNLLS-N, weighted NLLS using noisy tissue time-activity data; WNLLS-NF, weighted NLLS using noise-free tissue time–activity data.

on the variable's measurement unit. The higher the CV the greater the dispersion in the variable. Moreover, the average running time t for each method was calculated for comparison of computational efficiency.

For each noise level, 1000 realizations were run. Then these simulated data were fitted using these parameter estimation methods and criteria were calculated. All the calculations are run on a Windows-PC with an Intel Pentium4 3.4GHz processor (Santa Clara, California, USA) and a 2-gigabyte physical memory.

Results

Figures 1a–f and 2a–f show the box plots and the plots of the percentage bias versus CV of $K_1^*, k_2^*, k_3^*, k_4^*, V_b$ and *MRGlc* estimates obtained from the different methods at different noise levels. The scanning length is 120 min. Figures 3a–f and 4a–f show the results corresponding to the 60 min scan. As only MRGlc can be estimated for the PGA method, the individual rate constants are not available in the figures. In the box plots, the horizontal axis corresponds to the noise levels and the vertical axis corresponds to the parameter values. The individual boxes

Fig. 2

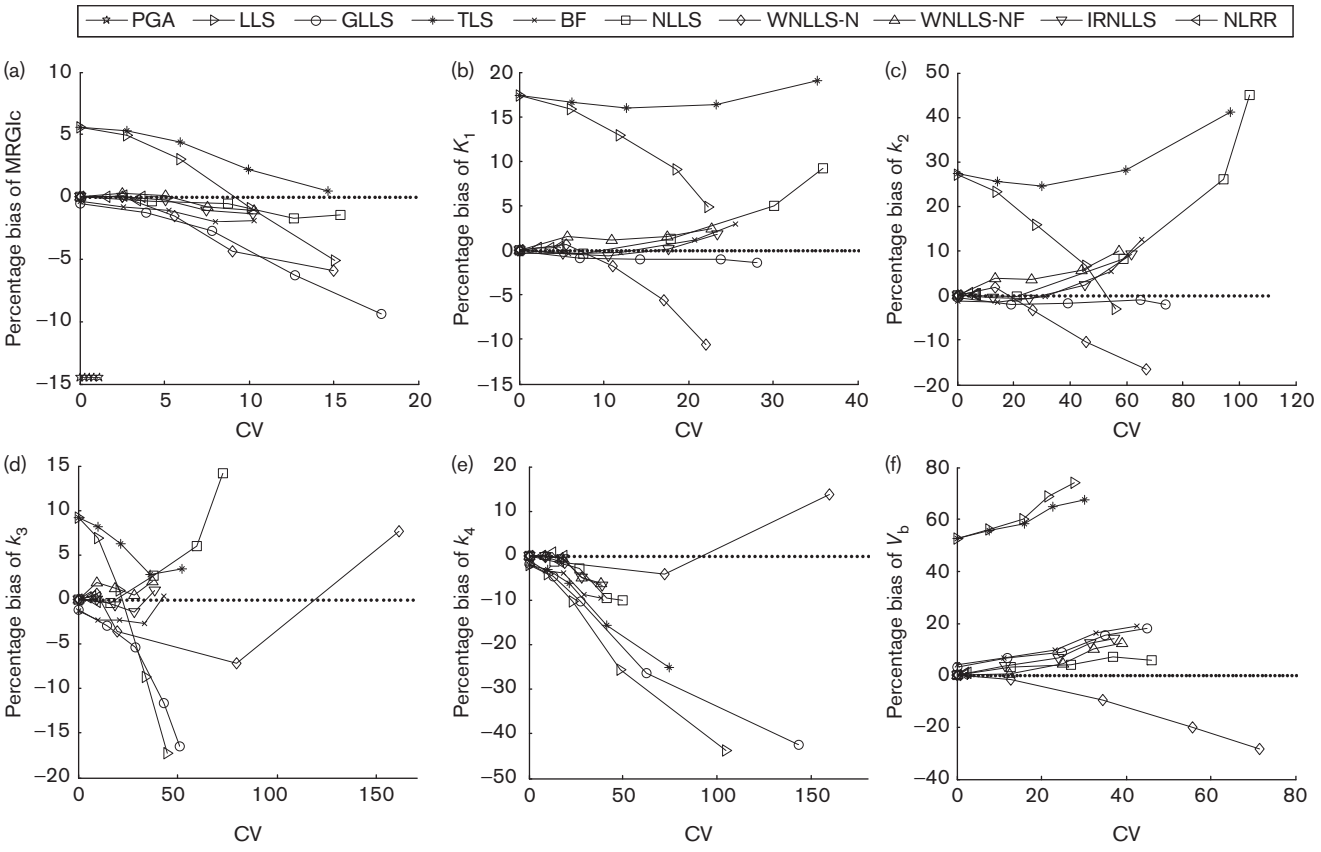

Plots of percentage bias versus coefficient of variation of (a)K_1^*, (b) k_2^*, (c) k_3^*, (d) k_4^*, (e) V_b, and (f) metabolic rate for glucose (MRGlc). The scanning length is 120 min. Different points for each method correspond to the different noise levels. BF, basis functions; GLLS, generalized linear least squares; IRWNLLS, iteratively reweighted nonlinear least squares; LLS, linear least squares; NLLS, nonlinear least squares; NLRR, nonlinear ridge regression; PGA, Patlak–Gjedde graphical analysis; TLS, total least squares;WNLLS-N, weighted NLLS using noisy tissue time-activity data; WNLLS-NF, weighted NLLS using noise-free tissue time-activity data.

have lines at the lower (25th percentile of the data), median (50th percentile of the data, indicated by a horizontal line within the box), and upper quartile values (75th percentile of the data). Thus, the box indicates where the middle 50% of the data are located. The whiskers extend from the ends of the box to the most extreme value with 1.5 times IQR in each direction. The estimates beyond the whiskers are marked by '+'. The true values for each parameter are also plotted for better comparison. In the plots of the percentage bias versus CVs, the horizontal dashed line in each subfigure indicates zero bias. The farther the points to the dashed line or the larger the CV values, the more biased or the less precise the estimation method would be. A good estimation method would have its point pairs (percentage bias, CV) around the origin (0,0) as close as possible.

In this study, the effect of different scanning schedules (120 min scan and 60 min scan) was investigated. From the results, generally the estimates obtained from each method with the 120 min scan are more accurate than those with the 60 min scan, especially at the high noise level. Linear squares methods (LLS, TLS, and GLLS) tend to be more easily affected by scanning lengths than the other methods. Moreover, the results also indicate that the precision of k_4^* is very poor with the 60 min scan, especially when estimated by linear squares methods (Figs 3d and 4e). The observation that k_4^* may not be determined reliably with the 60 min scan is consistent with earlier reports [25–27].

In Figs 1 and 3, when the data is noise free, all methods except PGA, LLS, and TLS show low bias as the estimates from these methods are very close to the true parameter values. Consistent with the observation in the literature published earlier, the assumption of $k_4^* = 0$ introduces bias for the PGA method [22,28]; it underestimates (Fig. 1f, 14.5% for 120 min) or overestimates (Fig. 3f, 7.8% for 60 min) the MRGlc. LLS and TLS overestimate all parameters (except k_4^* in Fig. 1d) in both the cases, suggesting that when solving nonlinear problems in the linear squares sense, bias exists even

Fig. 3

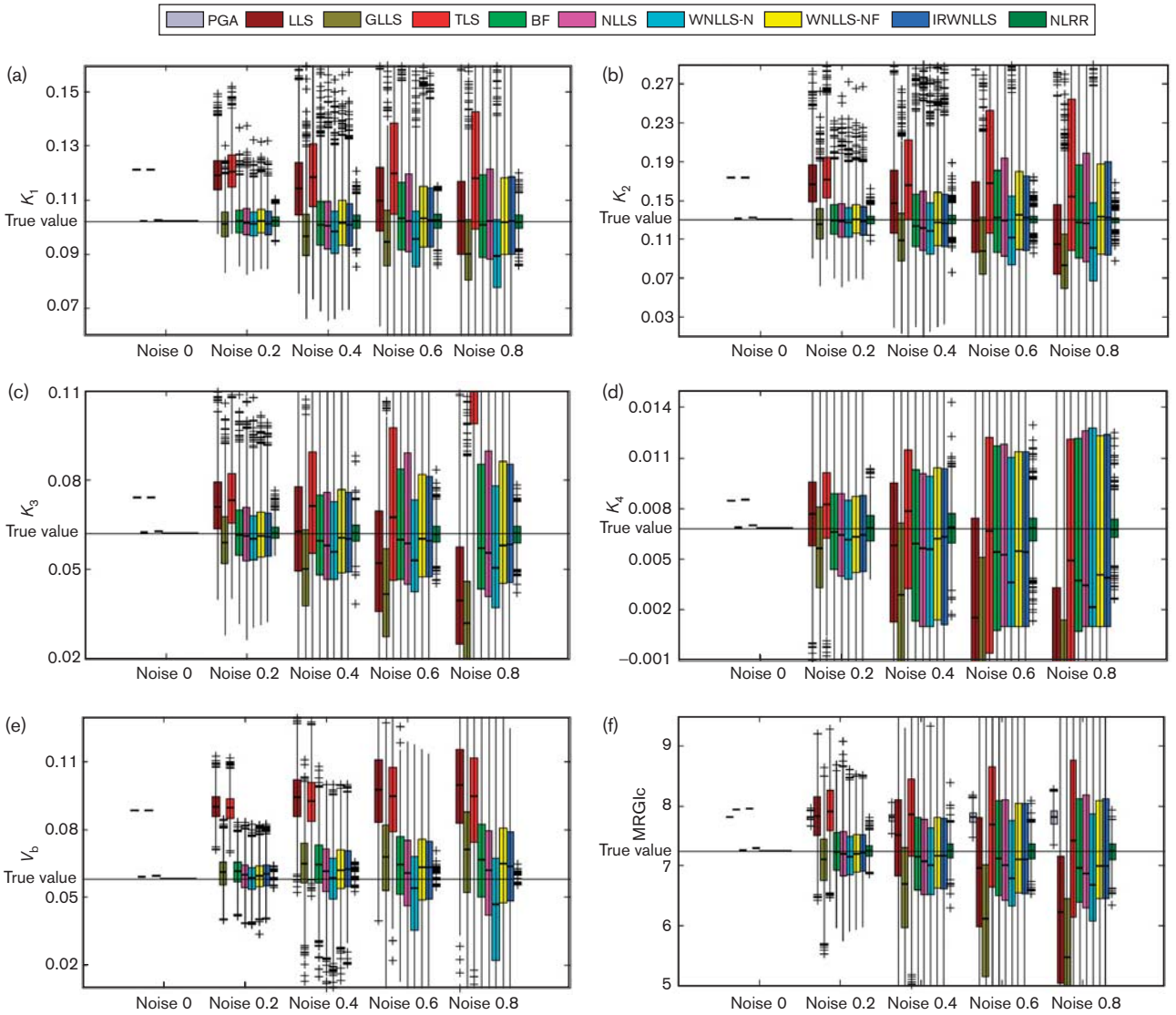

Box plots of (a)K_1^*, (b) k_2^*, (c) k_3^*, (d) k_4^*, (e) V_b, and (f) metabolic rate for glucose (MRGlc) estimates obtained with different methods at different noise levels. The scanning length is 60 min. The individual boxes have lines at the lower, median, and upper quartile values. The whiskers extend from the ends of the box to the most extreme value with 1.5 times the interquartile range in each direction. The estimates beyond the whiskers are marked as outliers (denoted by '+'). BF, basis functions; GLLS, generalized linear least squares; IRWNLLS, iteratively reweighted nonlinear least squares; LLS, linear least squares; NLLS, nonlinear least squares; NLRR, nonlinear ridge regression; PGA, Patlak–Gjedde graphical analysis; TLS, total least squares; WNLLS-N, weighted NLLS using noisy tissue time-activity data; WNLLS-NF, weighted NLLS using noise-free tissue time-activity data.

when fitting the noise-free data. GLLS and BF achieve lower bias (a small negative bias from −0.2 to −1.2% for each parameter) and higher precision than LLS and TLS at the lowest noise level. All nonlinear estimation methods tend to provide accurate estimates for each parameter.

At increasing noise levels, all methods tend to have poorer precision compared with their low noise level cases, as all the IQRs are increasing as shown in Figs 1 and 3. PGA is considered as the most stable method as its precision is little affected by noise, however, still with approximately 8–15% bias (Figs 1f, 2a, 3f and 4a). BF performs best in the category of linear estimation methods and even outperforms NLLS and WNLLS-N not only in its lower bias but also in its better precision (Figs 2 and 4). GLLS performs better than LLS and TLS at the low noise level; however, it exhibits large bias when the noise level is high especially in determining k_3^* (45% for 60 min) and k_4^* (42% for 120 min and even exceeded 200% for 60 min) (Figs 2d, e, 4d, e). LLS and TLS do not show regular improvement or deterioration in the accuracy of estimates with increasing noise levels. In the nonlinear estimation methods, NLRR shows the best bias and precision

Fig. 4

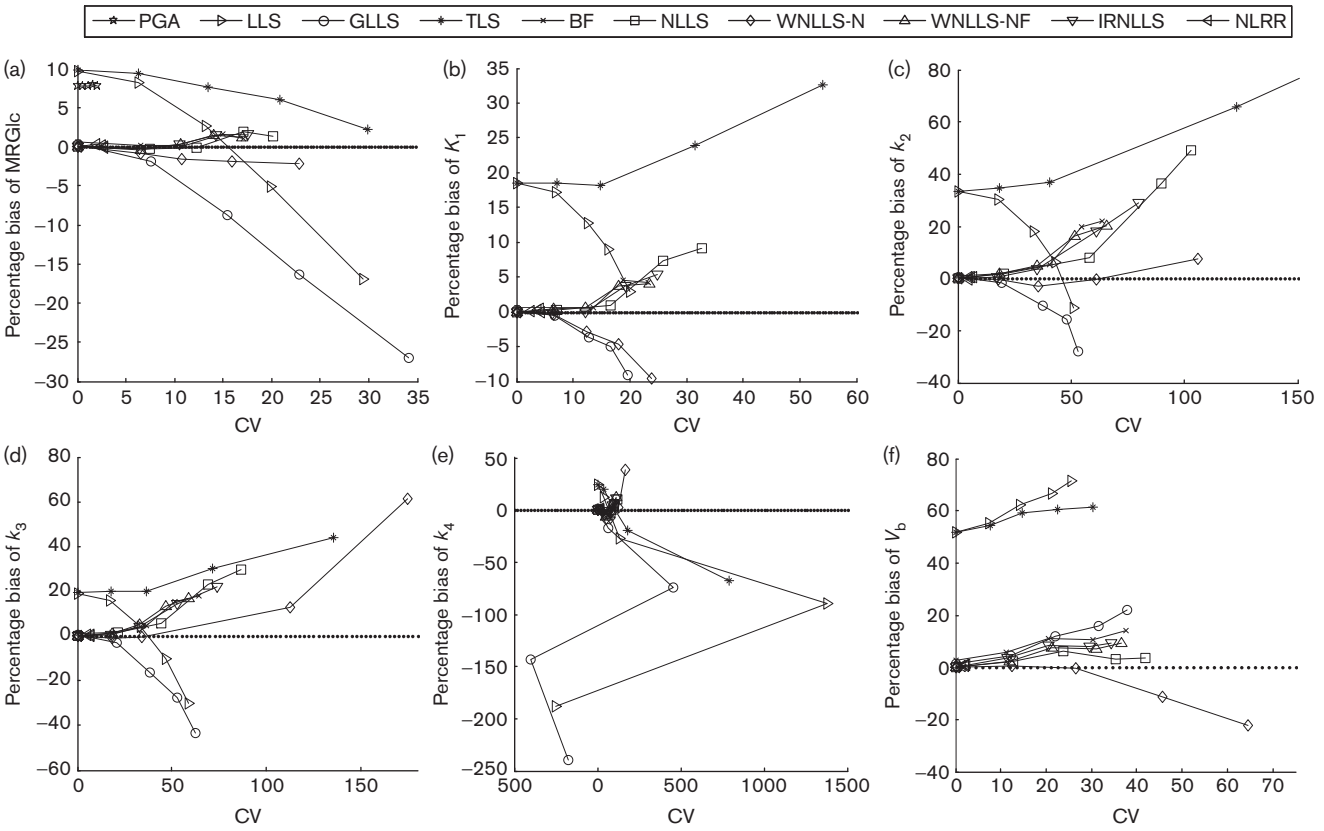

Plots of percentage bias versus CV of (a)K_1^*, (b) k_2^*, (c) k_3^*, (d) k_4^*, (e) V_b, and (f) metabolic rate for glucose (MRGlc). The scanning length is 60 min. Different points for each method correspond to the different noise levels. BF, basis functions; GLLS, generalized linear least squares; IRWNLLS, iteratively reweighted nonlinear least squares; LLS, linear least squares; NLLS, nonlinear least squares; NLRR, nonlinear ridge regression; PGA, Patlak–Gjedde graphical analysis; TLS, total least squares; WNLLS-N, weighted NLLS using noisy tissue time-activity data; WNLLS-NF, weighted NLLS using noise-free tissue time-activity data.

properties, whereas WNLLS-N shows the poorest properties with increasing noise levels. WNLLS-NF and IRWNLLS provide more reliable results than NLLS. This indicates the importance of the choice of weighting factors in the nonlinear estimation methods. As the gold standard method, NLLS exhibits low bias at the low noise level, but high bias and poor precision at the middle–high noise levels; for example, bias range of k_3^* is 2.6–14.2% for 120 min and 5.6–29.6% for 60 min, and range of k_4^* is −2.9 to −9.9% for 120 min and −3.5 to 10.3% for 60 min; CV values range of k_3^* is 38.1–72.7% for 120 min and 44.4–86.6% for 60 min, and of k_4^* is 27.2–50.1% for 120 min and 81.9–121.3% for 60 min.

For MRGlc in Figs 2a and 4a, the MRGlc estimates from the linear estimation methods, except BF, tend to be less accurate than those from the other methods; for K_1^* in Fig. 2b and Fig. 4b, LLS, TLS, NLLS, and WNLLS-N show more bias than GLLS, BF, WNLLS-NF, IRNLLS, and NLRR; for k_2^* in Fig. 2c and Fig. 4c, LLS, TLS, and NLLS generally exhibit larger bias; for k_3^* and k_4^* in Figs 2d, e, 4d, e, LLS, TLS, GLLS, and WNLLS-N tend to be more biased, with bias even exceeding 200% for k_4^* at noise level 0.6 and above with the 60 min scan (Fig. 4e); for V_b in Figs 2f 4f, LLS, TLS, and WNLLS-N exhibit higher bias than the other methods.

Figure 5 shows the average running time for each analysis method at the different noise levels. As the running time for the 120 min scan is almost the same as that for the 60 min scan, only one case is shown here. From the results, IRWNLLS was most time consuming (1–2 s), as it needed to iteratively adjust the weighting factors and fit the model. The time complexities of NLLS, WNLLS-N, and WNLLS-NF are in the same order of magnitude (0.6–0.8 s). GLLS and BF show slight superiority in running time (0.2–0.4 s) than the nonlinear estimation methods; however, they are more time consuming than the other linear estimation methods such as PGA, LLS, and TLS (0.005–0.007 s).

In general, most of the linear estimation methods are found to be more computationally efficient, whereas most of the nonlinear estimation methods tend to achieve

Fig. 5

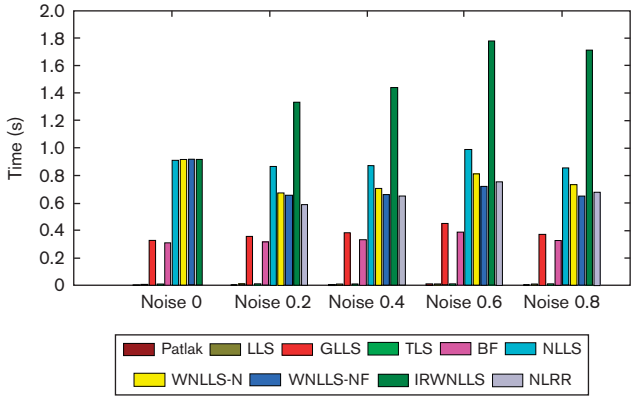

The average running time for each parameter estimation method. BF, basis functions; GLLS, generalized linear least squares; IRWNLLS, iteratively reweighted nonlinear least squares; LLS, linear least squares; NLLS, nonlinear least squares; NLRR, nonlinear ridge regression; PGA, Patlak–Gjedde graphical analysis; TLS, total least squares; WNLLS-N, weighted NLLS using noisy tissue time-activity data; WNLLS-NF, weighted NLLS using noise-free tissue time-activity data.

better accuracy. In the category of linear estimation methods, BF is the most promising method at the tradeoff between computational cost and estimation accuracy and precision. Moreover, BF is less influenced by the scan duration used. In the category of nonlinear estimation methods, from the perspective of accuracy and precision, the order of these methods (from best to worst) is NLRR, WNLLS-NF, IRWNLLS, NLLS, and WNLLS-N. However, as NLRR and WNLLS-NF use the true parameter values and the true noise variance as prior information that makes them impractical in clinical studies, and IRWNLLS is excessively time consuming, NLLS may be the most suitable method. When comparing BF with NLLS, it is shown that BF performs better than NLLS in terms of its statistical reliability and computational efficiency. Thus, if reliable parameter bounds (that can be determined from earlier studies) are known, then BF is the most preferred method.

Discussion

In dynamic ^{18}F-FDG PET imaging, several approaches to determine kinetic parameters have been proposed continuously in recent years. Some researchers have also evaluated some methods used in dynamic ^{18}F-FDG PET imaging [2,7,29,30]. However, these historical evaluations were not investigated under the same configuration, and some conclusions have led to some confusion in whether or how to best apply these methods. Moreover, only a subset of these estimation methods was included in each historical evaluation, and some recently proposed methods were not included for comparison. For example, Feng *et al.* [7] did not include the cerebral blood volume effect in the pharmacokinetic model, whose necessity has been shown by Lammertsma *et al.* [31] when the individual rate constants were to be determined, and they declared the superiority of GLLS; Muzic and Christian [2] focused their attention on evaluating objective functions used in iterative nonlinear estimation methods, and questioned the appropriateness of using GLLS in parametric imaging. In this study, several popular existing and newly developed linear and nonlinear estimation methods were systematically compared and evaluated in terms of their statistical reliability and computational efficiency under the same configuration while trying to clarify these confusions. The performance advantages and disadvantages of these methods were shown. Only simulation studies were presented as the true parameter values are known for accurate comparison. To better understand the results, besides the parameter set used for simulation in this study, we also tested another commonly used parameter set [22]: $K_1^* = 0.0540$, $k_2^* = 0.1090$, $k_3^* = 0.0450$, $k_4^* = 0.0058$, and $V_b = 0.025$. Similar results to those in this study were observed. The results are given in the supplementary figures.

In the category of linear estimation methods, PGA is found to achieve the best precision, however, to be markedly biased. The reason for its good precision is that fitting the PGA curve is restricted to the latter linear part of the curve (from 20 min onwards), which is less influenced by noise thus reducing the CV values. When applying PGA, two assumptions are made. First is complete equilibration between the tracer in the tissue and plasma, and second is the absence of metabolic product loss during an ^{18}F-FDG scan (i.e. $k_4^* = 0$). Violation of any assumption may cause nonlinearity of the curve. As the rate of dephosphorylation of ^{18}F-FDG - 6-phosphate (k_4^*) is included and assumed to be fixed in this study, the PGA plot tends to slightly curve downwards in the end, which results in bias. The use of a V_b correction within the kinetic compartmental model may be another reason for the bias of the PGA method. An

appropriate and careful choice of the time intervals after sufficient tracer equilibration and before significant product loss occurs, may reduce the possible bias, as shown in the literature publishes earlier [32,33]. For example, in the 120 min scan, restricting the upper time limit from 120 to 90 min would reduce the bias from 10–15% to 2.5–4.0%.

LLS performs better than TLS. However, both of them tend to be easily affected by scan length and noise. Estimates with the 60 min scan show larger bias than those with the 120 min scan, especially for k_3^* and k_4^*. On account of this, in this study, we do not recommend LLS and TLS to be applied when short scan durations are used. Bias was observed even when fitting noise-free data using these two estimation methods, likely because linearization may induce some bias and the existence of numerical error may also induce bias. Although LLS and TLS do not show superiority in terms of accuracy and precision when compared with the nonlinear estimation methods, they have absolute superiority in terms of computational speed. Thus, they might be preferred for generating parametric images on a voxel-by-voxel basis. Combining LLS or TLS with some constraints, such as clustering [34], ridge regression with spatial constraints [35] or other noise reduction strategies, will possibly remove part of the bias and improve the quality of the parametric images generated.

GLLS is a controversial method because of some inconsistent conclusions in earlier studies. There are several reports on the superiority of GLLS as 'an unbiased, computationally efficient algorithm' [7,11,36,37], whereas there are also some disagreements on the use of this method. Muzic and Christian [2] compared GLLS with other methods saying GLLS exhibited large bias even when fitting noise-free data 'bringing into question the appropriateness of using this method for parametric imaging'. Negoita and Renaut [38] discussed the convergence of GLLS and concluded that GLLS did not always converge to solve the nonlinear problem. In the study, GLLS outperforms LLS and achieves as low bias and high precision as the nonlinear estimation methods when the noise level is low, confirming that introducing an autoregressive filter in GLLS does help to improve the estimation accuracy, which is consistent with the observations of Feng *et al.* [7] in ^{18}F-FDG PET studies and Boellaard *et al.* [17] in ^{15}O-water PET studies. However, when the noise level is high, it exhibits large bias for each parameter (negative bias for $K_1^* - k_4^*$ and MRGlc, and positive bias for V_b), especially for k_3^* and k_4^*. The reason for its large bias at a high noise level may be that the noise would make iterative GLLS converge to a wrong solution, and whitening the correlated equation noise in LLS is not enough to overcome the detrimental effect of noise. Moreover, GLLS does not show obvious superiority in running time compared with nonlinear estimation methods. The computational cost of GLLS depends on the number of iterations. In this study, only two iterations are used as described by Feng *et al.* [11]. In each iteration, the discrete convolutions need to be calculated, which leads to resampling and interpolation of TTACs and PTAC, which makes GLLS much more time consuming. In general, if one wants to use GLLS to determine kinetic parameters, noise reduction strategies should be used to reduce the effect of noise, otherwise GLLS may not significantly reduce bias compared with LLS.

BF is a promising method that shows relatively low bias and high precision at each noise level. It outperforms all the other linear estimation methods and even performs better than the standard nonlinear estimation method NLLS. This finding is consistent with that of Hong and Fryer [21], who proposed this method and showed its superiority in both simulated and clinical studies. The majority of its computational cost is in the predefinition of the BF (10 000 BF in this study) that only need to be run once. Thus, the average running time would be reduced with the decreasing number of BF or increasing number of voxels to be processed. Therefore, BF is suitable for generating parametric images on the voxel-by-voxel basis. However, the parameter bounds used to construct BF may bring risk of bias. If the true parameter values are not included in the range of physiological values, which may happen in some abnormal tissue cases, large bias would arise. This possible disadvantage may partly be avoided by using a larger range of physiological values at the cost of increased running time. Thus, one should investigate this possible disadvantage of BF when applying it in individual applications.

In the category of nonlinear estimation methods, NLRR achieves the best precision. It is easy to understand as NLRR uses the true parameter values as prior information to construct the penalty function. The higher the degree of reliance to place on the penalty function, the more precise the estimated parameters would be. In this study, the reliance estimator τ is determined by a plug-in approach that proves to be efficient in this simulation study. However, as the true parameter values are unknown in practice, average parameter values obtained by applying NLLS on the smoothed images [3,4] are always used instead as prior information to construct the penalty function. This treatment improves the estimation precision compared with NLLS; however, it also has risks as the performance of NLRR relies on the NLLS estimates that could be biased. The greater the emphasis on prior knowledge, the more biased the NLRR estimates would be. Moreover, in such a case, the running time would be doubled as the NLLS is prerun to get the initial values.

For other nonlinear estimation methods, the most commonly used WNLLS-N performs the worst in all criteria. WNLLS-NF and IRWNLLS are always reliable at

each noise level, whereas NLLS gives acceptable performance. This indicates the importance of the choice of weighting factors. Weighting based on noisy experimental data should be avoided. Although the real noise-free data cannot be obtained in practice, IRWNLLS provides a method to iteratively approach the real noise variance to obtain the smallest variance of estimates. From the plots of percentage bias versus CVs, when the noise level is low, WNLLS-N, WNLLS-NF, and IRWNLLS have similar precision, suggesting that the noise in the data is too small to make any difference to the weighting factors to affect their performance. Meanwhile, the NLLS estimates have greater dispersion than these methods at the low noise level, suggesting that appropriate weighting could reduce the possibility of estimates being trapped in local minima and make the estimates more accurate. However, when the noise level is high, the WNLLS-N estimates have the largest bias and poorest precision in most cases, suggesting that when the data is noisy, inappropriate weighting is even inferior to uniform weighting. It is also suggested that if the noise variance is unknown in clinical applications, then NLLS is the best choice. The observation is consistent with that of Thiele and Buchert [39] in ^{11}C-(+)McN5652, ^{11}C-DASB, and ^{11}C-raclopride PET studies with the simplified reference tissue model.

Conclusion

In conclusion, there are several findings: (i) when the noise level is low, GLLS can achieve as low bias and high precision as the nonlinear estimation methods, but when the noise level is high it exhibits large bias especially in determining k_3^* and k_4^*. In addition, GLLS does not show an obvious advantage in running time. (ii) BF is a promising method with superior bias and precision properties, and is less affected by the scan duration used. It is suitable for determining kinetic parameters at the voxel level. PGA and LLS can be used to generate parametric images on a voxel-by-voxel basis because of their computational efficiency. However, if accurate estimates for all parameters are required, then BF is preferred at the cost of relatively increased computational time. (iii) The weighting factors in the nonlinear estimation methods are important because a good choice of weights can help to make the estimates more accurate and reliable. Weighting based on the noisy data should be avoided. If the noise variation is unknown, then NLLS is the recommended method. (iv) This study confirms that PGA is little affected by noise, but the assumptions of PGA could induce bias. It also confirms that 60 min is not long enough to give reliable estimates of k_4^* especially for linear squares methods LLS, TLS and GLLS.

Acknowledgements

This study is supported by the Project for the National Basic Research Program of China (973) under Grant No. 2011CB705700, the Changjiang Scholars and Innovative Research Team in University (PCSIRT) under Grant No. IRT0645, the CAS Hundred Talents Program, the Knowledge Innovation Project of the Chinese Academy of Sciences under Grant No. KSCX2-YW-R-262, KGCX2-YW-129, the National Natural Science Foundation of China under Grant Nos. 30873462, 60910006, 30970769, 30970771. The earlier part of this study has been published in the Proceedings of SPIE 2010.

References

1 Huang S, Phelps M, Hoffman E, Sideris K, Selin C, Kuhl D. Noninvasive determination of local cerebral metabolic rate of glucose in man. *Am J Physiol Endocrinol Metab* 1980; **238**:E69.
2 Muzic RF Jr, Christian BT. Evaluation of objective functions for estimation of kinetic parameters. *Med Phys* 2006; **33**:342.
3 Byrtek M, O'Sullivan F, Muzi M, Spence A. An adaptation of ridge regression for improved estimation of kinetic model parameters from PET studies. *IEEE Trans Nucl Sci* 2005; **52**:63–68.
4 O'Sullivan F, Saha A. Use of ridge regression for improved estimation of kinetic constants from PET data. *IEEE Trans Med Imaging* 1999; **18**:115–125.
5 Patlak C, Blasberg R. Graphical evaluation of blood-to-brain transfer constants from multiple-time uptake data. Generalizations. *J Cereb Blood Flow Metab* 1985; **5**:584.
6 Patlak CS, Blasberg RG, Fenstermacher JD. Graphical evaluation of blood-to-brain transfer constants from multiple-time uptake data. *J Cereb Blood Flow Metab* 1983; **3**:1–7.
7 Feng D, Ho D, Chen K, Wu LC, Wang JK, Liu RS, Yeh SH. An evaluation of the algorithms for determining local cerebral metabolic rates of glucose using positron emission tomography dynamic data. *IEEE Trans Med Imaging* 1995; **14**:697–710.
8 Blomqvist G. On the construction of functional maps in positron emission tomography. *J Cereb Blood Flow Metab* 1984; **4**:629.
9 Evans A, Diksic M, Yamamoto Y, Kato A, Dagher A, Redies C, Hakim A. Effect of vascular activity in the determination of rate constants for the uptake of ^{18}F-labeled 2-fluoro-2-deoxy-D-glucose: error analysis and normal values in older subjects. *J Cereb Blood Flow Metab* 1986; **6**:724–738.
10 Cai W, Feng D, Fulton R, Siu WC. Generalized linear least squares algorithms for modeling glucose metabolism in the human brain with corrections for vascular effects. *Comput Methods Programs Biomed* 2002; **68**:1–14.
11 Feng D, Huang SC, Wang ZZ, Ho D, An unbiased parametric imaging algorithm for nonuniformly sampled biomedical system parameter estimation. *IEEE Trans Med Imaging* 1996; **15**:512–518.
12 Van Huffel S, Vandewalle J. *The total least squares problem: computational aspects and analysis*. Philadelphia: Society for Industrial Mathematics; 1991.
13 Alspaugh J, Cao Y. SU-FF-J-91: linear methods for hepatic perfusion imaging. *Med Phys* 2006; **33**:2041.
14 Ichise M, Toyama H, Innis RB, Carson RE. Strategies to improve neuroreceptor parameter estimation by linear regression analysis. *J Cereb Blood Flow Metab* 2002; **22**:1271–1281.
15 Varga J, Szabo Z. Modified regression model for the Logan plot. *J Cereb Blood Flow Metab* 2002; **22**:240–244.
16 Cunningham V, Jones T. Spectral analysis of dynamic PET studies. *J Cereb Blood Flow Metab* 1993; **13**:15.
17 Boellaard R, Knaapen P, Rijbroek A, Luurtsema GJJ, Lammertsma AA. Evaluation of basis function and linear least squares methods for generating parametric blood flow images using ^{15}O-water and positron emission tomography. *Mol Imaging Biol* 2005; **7**:273–285.
18 Gunn RN, Lammertsma AA, Hume SP, Cunningham VJ. Parametric imaging of ligand-receptor binding in PET using a simplified reference region model. *Neuroimage* 1997; **6**:279–2787.
19 Lodge MA, Carson RE, Carrasquillo JA, Whatley M, Libutti SK, Bacharach SL. Parametric images of blood flow in oncology PET studies using [^{15}O] water. *J Nucl Med* 2000; **41**:1784.
20 Watabe H, Jino H, Kawachi N, Teramoto N, Hayashi T, Ohta Y, Iida H. Parametric imaging of myocardial blood flow with 15O-water and PET using the basis function method. *J Nucl Med* 2005; **46**:1219.
21 Hong YT, Fryer TD. Kinetic modelling using basis functions derived from two-tissue compartmental models with a plasma input function: general

principle and application to [(18)F]fluorodeoxyglucose positron emission tomography. *Neuroimage* 2010; **51**:164–172.
22 Phelps M, Huang S, Hoffman E, Selin C, Sokoloff L, Kuhl D. Tomographic measurement of local cerebral glucose metabolic rate in humans with (F-18) 2-fluoro-2-deoxy-D-glucose: validation of method. *Ann Neurol* 1979; **6**:371–388.
23 Logan J, Fowler JS, Volkow ND, Ding YS, Wang GJ, Alexoff DL. A strategy for removing the bias in the graphical analysis method. *J Cereb Blood Flow Metab* 2001; **21**:307–320.
24 Feng D, Huang S, Wang X. Models for computer simulation studies of input functions for tracer kinetic modeling with positron emission tomography. *Int J Biomed Comput* 1993; **32**:95.
25 Huang SC, Phelps M, Hoffman L, Kuhl D. Error sensitivity of fluorodeoxyglucose method for measurement of cerebral metabolic rate of glucose. *J Comput Assist Tomogr* 1982; **6**:860.
26 Jovkar S, Evans A, Diksic M, Nakai H, Yamamoto Y. Minimisation of parameter estimation errors in dynamic PET: choice of scanning schedules. *Phys Med Biol* 1989; **34**:895–908.
27 Zhou Y, Huang SC, Bergsneider M, Wong DF, Improved parametric image generation using spatial-temporal analysis of dynamic PET studies. *NeuroImage* 2002; **15**:697–707.
28 Guo H, Renaut RA, Chen K, Reiman E. FDG-PET parametric imaging by total variation minimization. *Comput Med Imaging Graph* 2009; **33**:295–303.
29 Krak NC, van der Hoeven JJM, Hoekstra OS, Twisk JWR, van der Wall E, Lammertsma AA. Measuring [^{18}F] FDG uptake in breast cancer during chemotherapy: comparison of analytical methods. *Eur J Nucl Med Mol Imaging* 2003; **30**:674–681.
30 Miyazawa H, Osmont A, Petit-Taboue M, Tillet I, Travere J, Young A, *et al.* Determination of ^{18}F-fluoro-2-deoxy-D-glucose rate constants in the anesthetized baboon brain with dynamic positron tomography. *J Neurosci Methods* 1993; **50**:263–272.
31 Lammertsma A, Brooks D, Frackowiak R, Beaney R, Herold S, Heather J, *et al.* Measurement of glucose utilisation with [^{18}F] 2-fluoro-2-deoxy-D-glucose: a comparison of different analytical methods. *J Cereb Blood Flow Metab* 1987; **7**:161.
32 Lucignani G, Schmidt KC, Moresco RM, Striano G, Colombo F, Sokoloff L, Fazio F. Measurement of regional cerebral glucose utilization with fluorine-18-FDG and PET in heterogeneous tissues: theoretical considerations and practical procedure. *J Nucl Med* 1993; **34**:360.
33 Schmidt KC, Lucignani G, Sokoloff L. Fluorine-18-fluorodeoxyglucose PET to determine regional cerebral glucose utilization: a re-examination. *J Nucl Med* 1996; **37**:394.
34 Huang X, Zhou Y, Bao S, Huang SC, Clustering-based linear least square fitting method for generation of parametric images in dynamic FDG PET studies. *Int J Biomed Imaging* 2007; **2007**. doi:10.1155/2007/65641.
35 Zhou Y, Huang SC, Bergsneider M. Linear ridge regression with spatial constraint for generation of parametric images in dynamic positron emission tomography studies. *IEEE Trans Nucl Sci* 2001; **48**:125.
36 Wen L, Eberl S, Feng D, Cai W, Bai J. Fast and reliable estimation of multiple parametric images using an integrated method for dynamic SPECT. *IEEE Trans Med Imaging* 2007; **26**:179–189.
37 Wong KP, Feng D, Siu WC. Generalized linear least squares algorithm for non-uniformly sampled biomedical system identification with possible repeated eigenvalues. *Comput Methods Programs Biomed* 1998; **57**:167–177.
38 Negoita C, Renaut RA. On the convergence of the generalized linear least squares algorithm. *BIT Numerical Math* 2005; **45**:137–158.
39 Thiele F, Buchert R. Evaluation of non-uniform weighting in non-linear regression for pharmacokinetic neuroreceptor modelling. *Nucl Med Commun* 2008; **29**:179.